Multi-point Scanning Two-photon Excitation Microscopy by Utilizing a High-peak-power 1042-nm Laser

Kohei OTOMO,[*1] **Terumasa HIBI,**[*1,*2] **Takashi MURATA,**[*3,*4] **Hirotaka WATANABE,**[*1,*2] **Ryosuke KAWAKAMI,**[*1,*2] **Hiroshi NAKAYAMA,**[*5] **Mitsuyasu HASEBE,**[*3,*4] **and Tomomi NEMOTO**[*1,*2†]

*1 *Research Institute for Electronic Science, Hokkaido University, Kita 20 Nishi 10, Kita, Sapporo 001-0020, Japan*
*2 *Graduate School of Information Science and Technology, Hokkaido University, Kita 14 Nishi 9, Kita, Sapporo 060-0814, Japan*
*3 *Division of Evolutionary Biology, National Institute for Basic Biology, Nishigonaka 38 Myodaiji-cho, Okazaki 444-8585, Japan*
*4 *Department of Basic Biology, School of Life Science, SOKENDAI (The Graduate University for Advanced Studies), Nishigonaka 38 Myodaiji-cho, Okazaki 444-8585, Japan*
*5 *Yokogawa Electric Corp., 2-3 Hokuyodai, Kanazawa 920-0177, Japan*

The temporal resolution of a two-photon excitation laser scanning microscopy (TPLSM) system is limited by the excitation laser beam's scanning speed. To improve the temporal resolution, the TPLSM system is equipped with a spinning-disk confocal scanning unit. However, the insufficient energy of a conventional Ti:sapphire laser source restricts the field of view (FOV) for TPLSM images to a narrow region. Therefore, we introduced a high-peak-power Yb-based laser in order to enlarge the FOV. This system provided three-dimensional imaging of a sufficiently deep and wide region of fixed mouse brain slices, clear four-dimensional imaging of actin dynamics in live mammalian cells and microtubule dynamics during mitosis and cytokinesis in live plant cells.

Keywords Two-photon excitation microscopy, multi-point laser scanning method, confocal microscopy, Yb-based laser

(Received December 24, 2014; Accepted February 14, 2015; Published April 10, 2015)

Introduction

Laser scanning microscopy utilizing two-photon excitation offers several advantages for biological imaging.[1] First, optically sectioned fluorescence images can be acquired because the excitation is spatially localized at the focus of the excitation laser light due to its non-linear dependence on the photon density. Second, the excitation laser light in the near-infrared (NIR) range enables a deeper penetration depth owing to a lower degree of absorption by living tissues. Thus, two-photon excitation laser scanning microscopy (TPLSM) has become an essential analytical method in life science and medical research.[2-8] Since most TPLSM systems employ a single-point laser scanning method using moving mirrors, their temporal resolution primarily depends on the speed of the physical movement of these mirrors. By utilizing resonant mirrors, video-rate scanning TPLSM has been achieved,[9] though the image quality was compromised for greater temporal resolution.

In contrast, multi-point laser scanning methods have attempted to improve the temporal resolution of a TPLSM system near the beginning of the 21st century.[10] As one of these methods, TPLSM that utilizes a spinning-disk scanner (TPLSM-SD) has been developed. At first, Bewersdorf *et al.* (1998) used a spinning micro-lens array disk to split the excitation light of a mode-locked Ti:sapphire (Ti:Sa) laser into an array of beams, and achieved video-rate TPLSM imaging.[11] Fujita *et al.* introduced a regenerative amplifier to increase the laser peak power, and achieved video-rate imaging over a wide field of view (FOV) using a 40× objective lens (NA 0.5).[12] The authors further combined a Nikpow disk that contained a set of confocal pinholes with a micro-lens array disk to capture confocal TPLSM images with improved spatial resolution.[13] Although those authors did not install an amplifier in this case, confocal pinholes improved the image spatial resolution and contrast by eliminating any undesirable fluorescence that is scattered or emitted by reabsorption in the specimen.[10,13] However, they found that the penetration depth and the FOV were limited due to a pair of spinning-disks, which reduced the Ti:Sa laser power.

The Confocal Scanning Unit (CSU) developed by Yokogawa Electric is a scanner that incorporates a micro-lens array disk and a Nipkow disk. The CSU enables the acquisition of confocal single-photon excitation fluorescent images; it is thus a popular tool for biological researchers to visualize any rapid movement of cellular structures.[14-16] In 2013, Shimozawa *et al.* reported that modifying the CSU's spinning-disk to increase the conventional Ti:Sa laser power throughput dramatically improved the TPLSM image quality.[17] They optimized the pinhole size, the distance between the pinholes and the

† To whom correspondence should be addressed.
E-mail: tn@es.hokudai.ac.jp

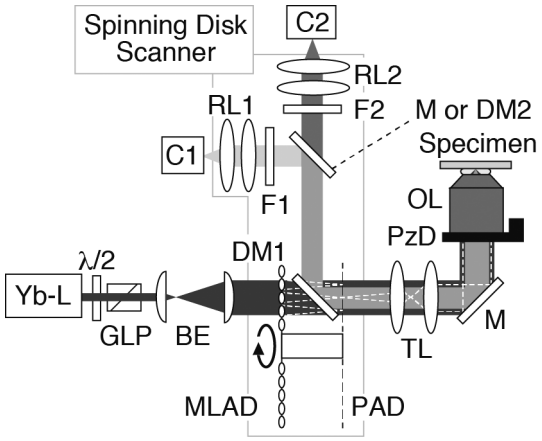

Fig. 1 Optical set-up of our two-photon excitation laser scanning microscope with a spinning-disk scanner (TPLSM-SD) system. BE: beam expander; C: camera; DM: dichroic mirror; F: filter; FM: flipper mount mirror; GLP: glan laser polariser; $\lambda/2$: half-wave plate; M: mirror; MLAD: micro-lens array disk; NC: negative chirper; OL: objective lens; PAD: pinhole array disk (Nipkow disk); PzD: piezo-z driver; RL: relay lenses; TL: tube lenses; Yb-L: Ytterbium-based laser.

corresponding micro-lenses aligned on the spinning-disk. They acquired optically sectioned TPLSM images of various biological specimens that were clearer than those acquired from one-photon excitation with the same fluorescence microscopy system. Clearer images resulted due to resolving the 'pinhole cross-talk' problem, wherein fluorescent signals from neighboring excitation points or out-of-focus planes enter a pinhole, and increase the background intensity.[17] However, since the power of a Ti:Sa laser was still insufficient, this TPLSM-SD system only used a 10% region of the effective area of the detector.[17]

In the present work, we installed a commercially available Ytterbium (Yb)-based laser with peak power 10-times greater than that of a Ti:Sa laser so as to enlarge the FOV for TPLSM-SD. This system provided three-dimensional (*xyz*) images of sufficiently wide, deep regions of fixed tissues, and clear four-dimensional (*xyz-t*) images of the living cell organelle microstructure.

Experimental

Optical set-up

A schematic of our optical set-up is shown in Fig. 1. Our TPLSM-SD system used a Yb-based laser (femtoTrain: 1042 nm, 10 MHz, 300 fs, 4.0 W; Spectra Physics, Santa Clara, CA) for two-photon excitation. The laser power was adjusted using a half wave-plate and a Glan-laser polariser. The beam width was enlarged by applying a beam expander comprising a pair of plano-convex lenses, resulting in more than a three-times larger width than that previously reported with a Ti:Sa laser beam.[17] This enlarged beam was introduced into a spinning-disk scanner with 100-μm-wide pinholes aligned on a Nipkow disk[17] (CSU-MPφ100; Yokogawa Electric, Kanazawa, Japan) installed on an inverted microscope (IX-71; Olympus, Tokyo, Japan). The incident excitation light was introduced at the pupil of the objective lens and focused on multiple points of a specimen. A water immersion lens (UPLSAPO60XW: NA = 1.20, WD = 0.28 mm; Olympus) or a silicone oil immersion lens (UPLSAPO30XS: NA = 1.05, WD = 0.80 mm; UPLSAPO60XS: NA = 1.30, WD = 0.30 mm; Olympus) was used. Fluorescent signals acquired by the objective lens were passed through the Nipkow disk and reflected by the first dichroic mirror (700 – 1100-nm band pass; Yokogawa Electric), passed through two infrared ray cut filters (FF01-770/SP-25 × 2; Semrock, Rochester, NY), and finally focused on the camera using relay lenses. A scientific complementary oxide semiconductor (sCMOS) camera (Neo: 2560 × 2160 pixels, pixel size: 6.5 μm × 6.5 μm; Andor Technology, Belfast, UK) or two EM-CCD cameras (iXon Ultra 897: 512 × 512 pixels, pixel size: 16 μm × 16 μm: Andor Technology, EM-C2: 1004 × 1002 pixels, pixel size: 8 μm × 8 μm; QImaging, Surrey, BC, Canada) were used, depending on the purpose.

A second dichroic mirror (600-nm long pass; Nikon, Tokyo, Japan) was placed in the optical path after the first dichroic mirror for two-color imaging. The transmitted fluorescent signals were passed through an infrared ray cut filter (SP880; Asahi Spectra, Tokyo, Japan) and a band-pass filter (590 – 644-nm band-pass; Yokogawa Electric), and then detected with one camera. Reflected fluorescent signals were passed through infrared ray cut filters (FF01-770/SP-25 × 2), and were detected with the other camera. The relay lenses were exchangeable, and magnification at ×1.2 or ×2 was selected, depending on the purpose. Z-scans were performed with either a piezo actuator (P-721; PI) or a focus drive motor (99A404; Ludl Electronic Products, Hawthorne, NY).

Non-biological sample preparation

Sulforhodamine B (SRB; Thermo Fisher Scientific, Rockford, IL) powder was dissolved in purified H_2O (final concentration, approximately 0.2 mM), and used to fill a glass-bottom dish so as to check the FOV of our TPLSM-SD system. Tiny fluorescent beads were mixed with 1% agarose gel (agarose L, Nippon Gene, Toyama, Japan). Yellow-green beads with diameters of 170 nm (170 nm yellow-green beads; Thermo Fisher Scientific) were used to evaluate the spatial resolution of our TPLSM-SD system.

Preparation of fixed brain slice specimens

An adult transgenic mouse (21-weeks of age) with enhanced yellow fluorescent protein (EYFP) (Thy1-YFP-H mouse; The Jackson Laboratory, Bar Harbor, ME) expression[18] was anaesthetised with pentobarbital sodium. The mouse was transcardially perfused with phosphate buffered saline (PBS; pH 7.4), followed by 4% formaldehyde. The brain was removed, incubated in PBS, and cortically cut with a vibratome (Vibrating Microtome 70000 smz; Campden Instruments Ltd., Loughborough, UK) into 900-μm-thick slices. The brain slices were treated with 60% 2,2′-thiodiethanol (TDE) in PBS (v/v) to clear the brain tissue.[19] All mice were housed on a 12:12 light–dark cycle (lights on from 8:00 to 20:00) with controlled temperature and humidity, and had ad libitum access to food and water.

All animal experiments were performed in accordance with the National University Corporation Hokkaido University Regulations on Animal Experimentation and the Guidelines for Proper Conduct of Animal Experiments (Science Council of Japan). This protocol was approved by the Institutional Animal Care and Use Committee of National University Corporation Hokkaido University (Permit Number: 10-0119).

Preparing plasmid DNA for expressing Lifeact-mCitrine expression

A plasmid harboring Lifeact[20] fused with mCitrine (EYFP with Q69M and A206K point mutations)[21,22] was constructed in

our laboratory, as briefly described below. A DNA fragment encoding for mCitrine was generated by a polymerase chain reaction. The pECFP-N1 plasmid (Clontech, Palo Alto, CA) was altered by substituting the ECFP coding region with that of mCitrine. Subsequently, the Lifeact coding region was inserted into this plasmid. The Lifeact-mCitrine coding region was sequenced and verified. Detailed methods and plasmid maps are available upon request.

HeLa cell culture and transfection

HeLa cells were cultured in Dulbecco's modified Eagle's medium (Wako Pure Chemical, Osaka, Japan), supplemented with 10% foetal bovine serum (FBS) and penicillin/streptomycin (Invitrogen, Carlsbad, CA) at 37°C with 5% CO_2. HeLa cells were seeded on a glass-bottom dish for observations,. Transfection with the Lifeact-mCitrine expressing plasmid was performed using FuGENE 6 (Promega, Madison, WI) according to the manufacturer's instructions. After incubation for one day, the culture medium was completely changed to Dulbecco's modified Eagle's medium without phenol red (Wako Pure Chemical), containing 10% FBS and antibiotics.

Living tobacco BY-2 cell sample preparation

The plasmid harboring EYFP-β-tubulin[23] for the stable transformation of tobacco BY-2 cells was a gift from Dr. Yasuhara (Kansai University, Osaka, Japan). *Agrobacterium*-mediated transformation of tobacco BY-2 cells was performed as previously described.[24] Transformed cells were subcultured every week in a modified LS medium.[25] The cells were attached to a glass-bottom dish, as previously described.[26]

Results and Discussion

FOV and point spread function (PSF) evaluations

We first checked the FOV of our TPLSM-SD system by acquiring images of an SRB solution that was used to fill in a glass-bottom dish (Fig. 2a). We used an sCMOS camera, which had the largest effective detection area among the cameras that we used. The dashed circle shown in Fig. 2a is the previously reported FOV size.[17] By estimating the full width at half maximum (FWHM) values from the fluorescent intensity profiles of the major and minor axes, the FOV of our system utilizing a Yb-based laser was approximately 10-times greater in area than that of the previous study. The square with the dotted line in Fig. 2a indicates the effective region of the iXon Ultra 897 EM-CCD camera. The effective region of the other EM-CCD camera (EM-C2) was 3.5% smaller than that of the iXon Ultra 897. As judged by the SRB solution images, the beam width of the Yb-based laser beam was appropriate for use with the area provided by the EM-CCD cameras, which corresponds to the square indicated in Fig. 2a. However, as shown in Figs. 2b and 2c, the fluorescence intensity ratios of the center to the edge of the FOV differed by two to three times because of the distribution of the irradiation excitation beam intensity. A flat-top beam made by a laser with increased power, coupled with a higher sensitivity camera, will be helpful for future improvements.

Additionally, we estimated the spatial resolution of our system from images of fluorescent beads smaller than the diffraction limit (Fig. 2d). The average ± standard deviation of the FWHM values along the *x*-, *y*- and *z*-axes using an objective lens with an NA of 1.30 were 338 ± 7, 314 ± 2 and 616 ± 21 nm, respectively (n = 5). Since the intensity distribution in the focal plane is generally slightly elongated along the polarized direction, the longer FWHM values for the *x*-axis than those for the *y*-axis reflect the polarization properties of the excitation light. To compare these values with the ideal two-photon excitation light focal pattern, we numerically calculated the square values of the intensity distributions around the ideal focal pattern of 1042-nm light polarized linearly along the *x*-axis using an objective lens with an NA of 1.30. The FWHM values of the *x*, *y*, and *z*-axes were 404, 307 and 823 nm, respectively. These values were larger than our measured values, particularly along the longitudinal axis. This improvement may have resulted from

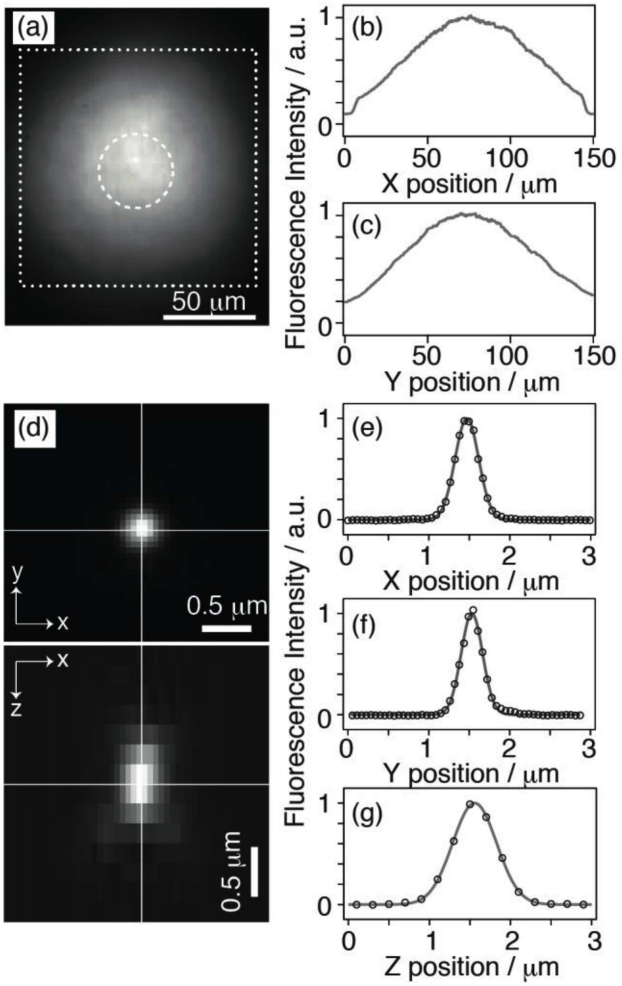

Fig. 2 Field of view (FOV) and point spread function (PSF) confirmation of our two-photon excitation laser scanning microscope with a spinning-disk scanner (TPLSM-SD) system. (a) Fluorescent images of a sulforhodamine B solution in a glass-bottom dish. The area shown corresponds to the window between the spinning-disk scanner and the microscope. An area 40 μm in diameter is superimposed at the center of this image with a dashed line to indicate the FOV area previously achieved by Shimozawa *et al.*[17] The square with the dotted line indicates the effective region of the iXon Ultra 897 EM-CCD camera. The right panels show the fluorescence intensity profiles across the intensity center along the *x*- and *y*-axes (b, c). Objective lens: UPLSAPO60XW. Relay lenses: ×1.2. Camera: Neo. Square with dotted lines indicates the effective region of the EM-CCD camera used (iXon Ultra 897). (d) Fluorescent images of a 170-nm YG bead. Images were reconstructed from z-stacks (2.8 μm thick) at 0.2-μm intervals. Objective lens: UPLSAPO60XS. Relay lenses: ×2. Camera: Neo. Right panels show the fluorescence intensity profiles across the intensity center along the *x*-, *y*- and *z*-axes (e – g). Circles and solid lines indicate measured values and fitted curves, respectively.

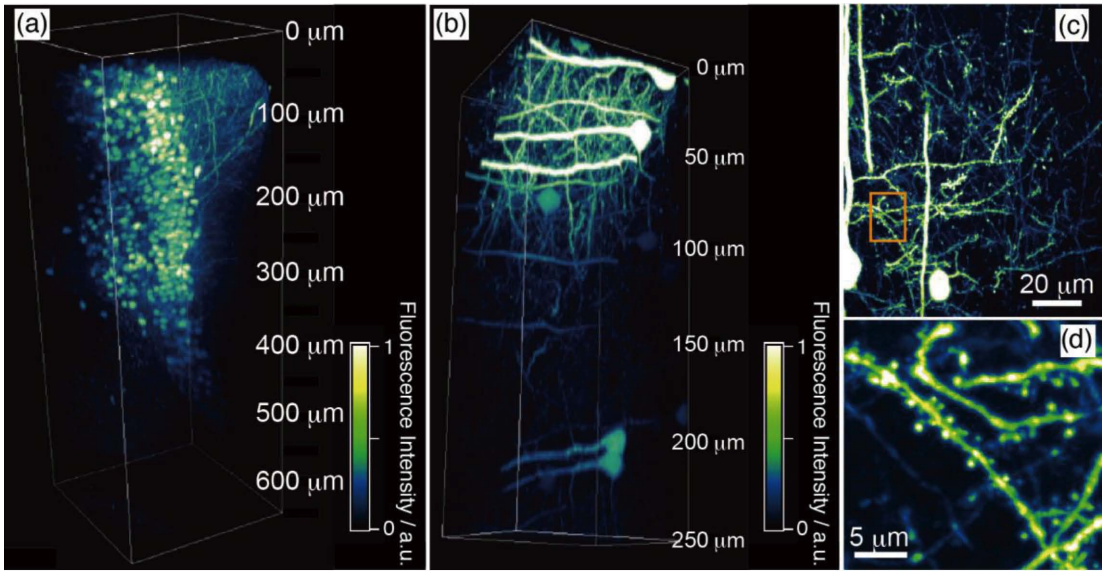

Fig. 3 Coronal sections (900 μm thick) from a Thy1-yellow fluorescent protein (YFP)-H mouse after treatment with a 60% 2,2′-thiodiethanol (TDE) clearing solution. (a) Images of granule cells in the hippocampal dentate gyrus reconstructed from z-stacks (650 μm thick) at 2.5-μm intervals. The exposure time was 500 ms, and the total time for acquiring the *xyz* image was 175 s. Objective lens: UPLSAPO30XS. Relay lenses: ×1.2. Camera: EM-C2. (b) Images of cortical layer V pyramidal neurons reconstructed from z-stacks (250 μm thick) at 0.5-μm intervals (c). Exposure time was 500 ms, and the total time to acquire the *xyz* image was 315 s. Objective lens: UPLSAPO60XS. Relay lenses: ×1.2. Camera: EM-C2. A maximum intensity projection image 6 – 21 μm deep is shown in (c). Z-stack construction image in (d) obtained for the area indicated by the orange rectangle in (c).

the confocal pinholes aligned on the Nipkow disk for the fluorescent light optical path, as discussed previously.[10,13,17]

XYZ imaging of neurons in fixed mouse brain slices prepared with a clearing technique

To demonstrate cross-sectional deep imaging using our TPLSM-SD system, we acquired *xyz* images of cleared brain slice samples from transgenic mice in which EYFP was expressed in their neurons. The clearing treatment consisted of immersing the specimens in a 60% TDE solution.[19] Thus, we used silicone fluid immersion lenses, as follows, to reduce the refractive index mismatch between the specimens (1.45) and the silicone fluid immersion medium (1.40) used for the objective lens. We first used a 30× objective lens (UPLSAPO30XS) because of its long working distance. As shown in Fig. 3a, this system provided *xyz* imaging of individual neurons in a fixed mouse brain slice within a sufficiently deep and wide region. Each granule cell in the hippocampal dentate gyrus was separately visualized at a 500-μm depth. Even after extending the acquisition time, individual neurons were not observed at depths > 650 μm, indicating that excitable fluorophores may not have been located there.

Next, we used a 60× objective lens (UPLSAPO60XS) owing to its high numerical aperture (NA 1.30). As shown in Fig. 3b, we acquired an *xyz* image of cortical neurons in a fixed mice brain slice within the working distance of this objective lens. The maximum intensity projection image of a nearby surface (15-μm thickness) was processed (Fig. 3c), and numerous minute structures were visualized in the entire FOV. As shown in Fig. 3d, further zoom-up revealed the fine structure of dendritic spines of pyramidal neurons.

XYZ-T imaging of living mammalian cells

To confirm that our TPLSM-SD system could capture the movement in living biological samples, the three-dimensional F-actin structure in living HeLa cells was visualized using Lifeact[20] fused with mCitrine. We acquired an optically sectioned image of this specimen with a sufficient fluorescent signal in 120 ms. Our system visualized an entire living cell for 3.7 s per *xyz* image when combined with a high-speed piezo-z driver (Fig. 4a). Time-lapse images of F-actin dynamics are shown in Figs. 4b – 4g and Movie S1 (Supporting Information). As indicated by the arrowheads in Figs. 4b – 4g, three-dimensional filopodia movement at the edge and the surface of a cell was traced in detail.

XYZ-T imaging of living plant cells

Furthermore, we used our TPLSM-SD system to visualize intracellular movement in plant cells, which are larger than HeLa cells. We observed tubulin dynamics in tobacco BY-2 cells during mitosis and cytokinesis, and visualized the microtubule redistributions using *xyz-t* imaging. Thirty-three optically sectioned fluorescent images of BY-2 cells that stably expressed EYFP-β-tubulin were acquired at 15-s intervals during mitosis over a 20 – 30 min period. As shown in Figs. 5a – 5c, our TPLSM-SD system visualized the redistribution of microtubules into the nuclear area when the nuclear membrane was collapsed.

We acquired two-color TPLSM-SD images on the basis of the property that a single wavelength of two-photon excitation laser excites fluorochromes over a wide range of excitation wavelengths.[2,7,28] BY-2 cells expressing EYFP-β-tubulin were stained with FM4-64 dye, and three-dimensional and two-color images were captured with 1042-nm two-photon excitation. A cell plate stained with FM4-64 and surrounding microtubules

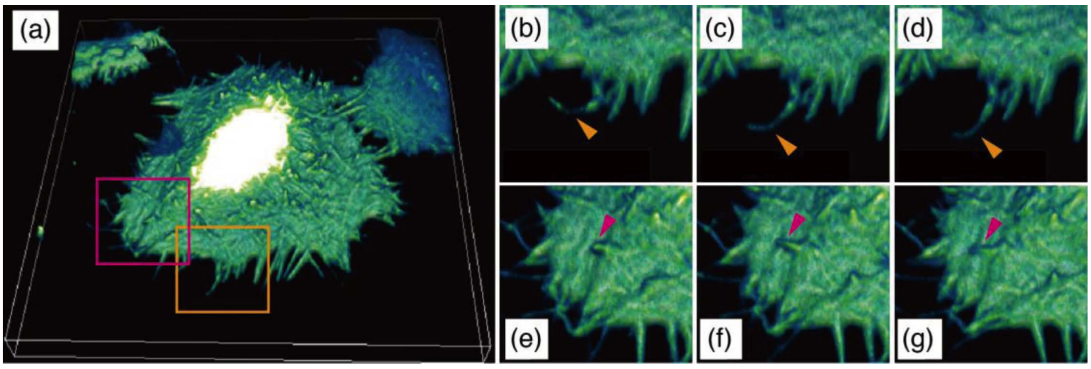

Fig. 4 Actin dynamics in HeLa cells expressing Lifeact-tagged mCitrine. Images were reconstructed from z-stacks (8 µm thick) at 0.5-µm intervals and shown in the shaded view. (a) An *xyz* image using the camera's entire field of view. Time-lapse images shown in (b – d) and (e – f) were obtained from the area indicated by the orange rectangle in (a) at 10 s per frame and a magenta rectangle in (a) at 20 s per frame. The exposure time was 120 ms, and the total time to acquire the *xyz* image was 3.7 s. Objective lens: UPLSAPO60XW. Relay lenses: ×1.2. Camera: iXon Ultra 897.

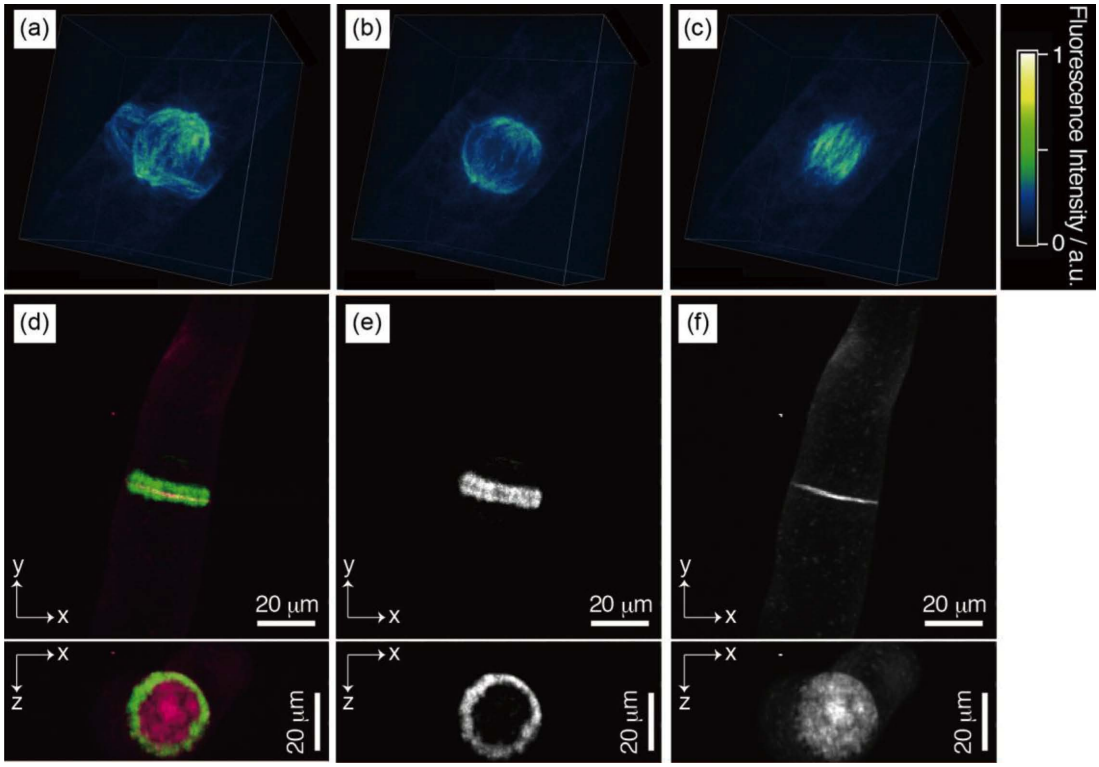

Fig. 5 (a – c) Mitotic spindle formation in a tobacco BY-2 cell expressing yellow fluorescent protein (EYFP)-β-tubulin. Images were reconstructed from z-stacks (33 µm thick) at 0.5-µm intervals. The images acquired at 0, 270 and 495 s after starting image acquisition are shown in (a), (b) and (c), respectively. The exposure time was 130 ms and the three-dimensional time lapse interval was 15 s. Objective lens: UPLSAPO60XW. Relay lenses: ×1.2. Camera: EM-C2 (binning 2 × 2). (d) Tobacco BY-2 cell undergoing cytokinesis and labeled with enhanced yellow fluorescent protein (EYFP)-β-tubulin (green) and FM4-64 (magenta). Images were reconstructed from z-stacks (40 µm thick) at 0.5-µm intervals. The exposure times for acquiring EYFP (e) and FM4-64 (f) fluorescent signals were 180 and 60 ms, respectively. The total time for *xyz* image acquisition was 20 s. The upper and lower panels show *xy* and *xz* views, respectively. Objective lens: UPLSAPO60XW. Relay lenses: ×1.2. Camera: iXon Ultra 897 × 2.

detected with EYFP-β-tubulin were visualized in separate channels (Figs. 5d – 5f and Movie S2 (Supporting Information)).

TPLSM-SD excitation laser light

In this study, we constructed a new TPLSM-SD system with a high-peak-power Yb-based laser light source. This system

enlarged the FOV by approximately 10-times more than that of previous systems using a conventional Ti:Sa laser light source. We confirmed that this system enabled the visualization of clear biological structures. A sufficient penetration depth and high spatiotemporal resolution were achieved by utilizing the larger FOV of this TPLSM-SD, making it suitable for visualizing a number of biological phenomena.

The high-peak-power laser used in this study cannot be used for high-speed scanning for single-point TPLSM. High-speed imaging with single-point TPLSM requires a high repetition rate laser light source due to the short pixel dwell time. For example, the pixel dwell time is approximately 0.125 µs during video-rate imaging with the single-point TPLSM with 512×512 pixels. Because our Yb-based laser irradiates once every 0.1 µs, only one or two laser pulses are used for each pixel when our laser is applied to the single-point TPLSM using a resonant scanner,[9] thus, uneven images could be acquired in this case. In contrast, the spinning-disk unit scanned a specimen with approximately 200 excitation beams, and the entire FOV was scanned once per half rotation of the spinning-disks (5 ms at 6000 rpm; the scanning properties of CSU-MPφ100 were different from the other CSU series due to modification of disks). Namely, approximately 10 million pulses were used for two-photon excitation within one scan run. Therefore, our measurement conditions might be sufficient to acquire a video-rate image.

Yb-based laser light at 1042-nm cannot excite green fluorescent protein (GFP) or fluorescent proteins with shorter excitation wavelengths, although these proteins are frequently used as cell markers and functional probes.[2] Thus, we developed a conventional Ti:Sa laser-based system, and attempted to increase the two-photon excitation probabilities of these proteins by introducing a negative chirper. Pulse compression increased the fluorescent signals by two to four times when using the Ti:Sa laser, depending on its oscillating wavelength (Fig. S1, Supporting Information). However, this TPLSM did not use the whole effective area of the detector due to an insufficient fluorescent signal. Developing a new laser with high-peak-power and a shorter wavelength is necessary when using GFP and other fluorescent proteins with shorter wavelength.

Choice of cameras

A multi-point laser scanning microscopy system uses cameras as detectors to simultaneously capture fluorescent signals from many focal points. Therefore, the image quality and temporal resolution largely depend on the sensitivities of the cameras used. We used an sCMOS camera and an EM-CCD camera with smaller pixel sizes for higher spatial resolution (Figs. 2d and 3). On the other hand, the latest EM-CCD camera, iXon Ultra 897, was used for shorter-time acquisition (Figs. 4 and 5d – 5f). Easy camera replacement is an advantage of this system because future technical developments of EM-CCD and sCMOS cameras will significantly improve the performance of this microscopy system.

In conclusion, we have shown that installing a Yb-based laser into a TPLSM-SD system significantly improved the FOV. Further improvements, including homogeneous image fields and applications to GFP, are expected along with developments in laser and camera technology.

Acknowledgements

We thank Dr. Y. Kozawa and Professor S. Sato of Institute of Multidisciplinary Research for Advanced Materials, Tohoku University for providing the program that numerically calculates the intensity distributions around an ideal light focal pattern, Dr. K. Kobayashi and Dr. Y. Matsuo of the Nikon Imaging Center at Hokkaido University for providing their technical support, and Dr. H. Yasuhara of Kansai University for providing EYFP-β-tubulin expressing plasmid. We are also grateful for the technical assistance provided by Ms. E. Ito, Ms. M. Oguro, Ms. S. Ipponjima, Mr. H. Osanai and Mr. R. Kitamura as well as the helpful advice of Dr. K. Iijima of the Laboratory of Molecular and Cellular Biophysics in the Research Institute for Electronic Science, Hokkaido University. This study was supported by JSPS KAKENHI (Grants Numbers 25840044, 25560411, 22300131, 22113005 and 26242082) of the Ministry of Education, Culture, Sports, Science and Technology (MEXT), Japan; by Orion research project (Okazaki Institute for Integrative Bioscience); by National Institute for Basic Biology; by the Nano-Macro Materials, Devices and System Research Alliance (MEXT) and by the Network Joint Research Center for Materials and Devices (MEXT).

References

1. W. Denk, J. H. Strickler, and W. W. Webb, *Science*, **1990**, *248*, 73.
2. M. Drobizhev, N. S. Makarov, S. E. Tillo, T. E. Hughes, and A. Rebane, *Nat. Methods*, **2011**, *8*, 393.
3. M. Matsuzaki, G. C. R. Ellis-Davies, T. Nemoto, Y. Miyashita, M. Iino, and H. Kasai, *Nat. Neurosci.*, **2001**, *4*, 1086.
4. T. Nemoto, R. Kimura, K. Ito, A. Tachikawa, Y. Miyashima, M. Iino, and H. Kasai, *Nat. Cell Biol.*, **2001**, *3*, 253.
5. E. Hirata, H. Yukigawa, Y. Kamioka, Y. Arakawa, S. Miyamoto, T. Okada, E. Sahai, and M. Matsuda, *J. Cell Sci.*, **2012**, *125*, 858.
6. S. Koga, Y. Oshima, N. Honkura, T. Iimura, K. Kameda, K. Sato, M. Yoshida, Y. Yamamoto, Y. Watanabe, A. Hikita, and T. Imamura, *Cancer Sci.*, **2014**, *105*, 1299.
7. R. Kawakami, K. Sawada, A. Sato, T. Hibi, Y. Kozawa, S. Sato, H. Yokoyama, and T. Nemoto, *Sci. Rep.*, **2013**, *3*, 1014.
8. T. Nemoto, *Mol. Cells*, **2008**, *26*, 113.
9. G. Y. Fan, H. Fujisaki, A. Miyawaki, R. K. Tsay, R. Y. Tsien, and M. H. Ellisman, *Biophys. J.*, **1999**, *76*, 2412.
10. J. Bewersdorf, A. Egner, and S. W. Hell, "*Handbook of Biological Confocal Microscopy*", ed. J. B. Pawley, **2006**, 3rd ed., Springer Science + Business Media, New York, 550.
11. J. Bewersdorf, R. Pick, and S. W. Hell, *Opt. Lett.*, **1998**, *23*, 655.
12. K. Fujita, O. Nakamura, T. Kaneko, S. Kawata, M. Oyamada, and T. Takamatsu, *J. Microsc.*, **1999**, *194*, 528.
13. K. Fujita, O. Nakamura, T. Kaneko, M. Oyamada, T. Takamatsu, and S. Kawata, *Opt. Commun.*, **2000**, *174*, 7.
14. T. Hama, A. Takahashi, A. Ichihara, and T. Takamatsu, *Cell. Signalling*, **1998**, *10*, 331.
15. K. Saito, Y. Arai, J. Zhang, K. Kobayashi, T. Tani, and T. Nagai, *Cell. Struct. Funct.*, **2011**, *36*, 237.
16. T. Murata, T. Sano, M. Sasabe, S. Nonaka, T. Higashiyama, S. Hasegawa, Y. Machida, and M. Hasebe, *Nat. Commun.*, **2013**, *4*, 1967.
17. T. Shimozawa, K. Yamagata, T. Kondo, S. Hayashi, A. Shitamukai, D. Konno, F. Matsuzaki, J. Takayama, S. Onami, H. Nakayama, Y. Kosugi, T. M. Watanabe, K. Fujita, and Y. Mimori-Kiyosue, *Proc. Natl. Acad. Sci. U. S. A.*, **2013**, *110*, 3399.

18. G. Feng, R. H. Mellor, M. Bernstein, C. Keller-Peck, Q. T. Nguyen, M. Wallace, J. M. Nerbonne, J. W. Lichtman, and J. R. Sanes, *Neuron*, **2000**, *28*, 41.
19. Y. Aoyagi, R. Kawakami, H. Osanai, T. Hibi, and T. Nemoto, *PLoS One*, in press.
20. J. Riedl, A. H. Crevenna, K. Kessenbrock, J. H. Yu, D. Neukirchen, M. Bista, F. Bradke, D. Jenne, T. A. Holak, Z. Werb, M. Sixt, and R. Weldlich-Soldner, *Nat. Methods*, **2008**, *5*, 605.
21. O. Griesbeck, G. S. Baird, R. E. Campbell, D. A. Zacharias, and R. Y. Tsien, *J. Biol. Chem.*, **2001**, *276*, 29188.
22. N. C. Shaner, P. A. Steinbach, and R. Y. Tisen, *Nat. Methods*, **2005**, *2*, 905.
23. H. Yasuhara and Y. Oe, *Protoplasma*, **2011**, *248*, 493.
24. G. H. An, *Plant Physiol.*, **1985**, *79*, 568.
25. T. Nagata, Y. Nemoto, and S. Hasegawa, *Int. Rev. Cytol.*, **1992**, *132*, 1.
26. T. Murata and T. I. Baskin, *Methods Mol. Biol.*, **2013**, *1136*, 47.
27. F. Kumagai, A. Yoneda, T. Tomida, T. Sano, T. Nagata, and S. Hasezawa, *Plant Cell Physiol.*, **2001**, *42*, 723.
28. S. Ogata, T. Miki, S. Seino, S. Tamai, H. Kasai, and T. Nemoto, *PLoS One*, **2012**, *7*, e37048.